



Universiteit
Leiden
The Netherlands

Graphene at fluidic interfaces

Belyaeva, L.A.

Citation

Belyaeva, L. A. (2019, October 23). *Graphene at fluidic interfaces*. Retrieved from <https://hdl.handle.net/1887/79822>

Version: Publisher's Version

License: [Licence agreement concerning inclusion of doctoral thesis in the Institutional Repository of the University of Leiden](#)

Downloaded from: <https://hdl.handle.net/1887/79822>

Note: To cite this publication please use the final published version (if applicable).

Cover Page



Universiteit Leiden



The handle <http://hdl.handle.net/1887/79822> holds various files of this Leiden University dissertation.

Author: Belyaeva, L.A.

Title: Graphene at fluidic interfaces

Issue Date: 2019-10-23

CHAPTER 1

Introduction

Graphene is a two dimensional (2D) allotrope of carbon, in which carbon atoms are packed in a hexagonal crystalline lattice.¹ Each carbon atom has four outer electrons, the s , p_x , and p_y orbitals which all participate in sp^2 hybridization and form three σ bonds with three neighbor atoms, and the electron on the p_z orbital forms a π bond. The π bonds result in an extended conjugated aromatic system over the entire graphene layer. Such electronic structure and, particularly, the π and π^* bands give rise to the diversity of graphene's remarkable electronic properties.² First, ideal graphene is a zero-gap semiconductor, or a semimetal, with the valence and conductance bands meeting at the Dirac points (Figure 1.1a).^{2,3} Unlike most semiconductors, graphene exhibits a linear energy dispersion relation (and, therefore, conical valence and conductance bands as opposed to parabolic, see Figure 1.1a), which implies that electrons are massless (or Dirac electrons, *i.e.* obeying the Dirac equation) and behave relativistically, moving with a speed close to the speed of light.^{2,3} Additionally, graphene shows outstanding hole and electron mobilities, reaching $15000 \text{ cm}^2 \text{ V}^{-1} \text{ s}^{-1}$ at room temperature.⁴ Anomalous Hall effect is another notable consequence of the unique electronic properties of graphene.⁵⁻⁷ Separately, the network of covalent C-C bonds makes graphene the strongest material, with a reported tensile strength of 130.5 GPa and a Young modulus of 1 TPa.⁸ Graphene is intrinsically rippled, with out-of-plane deformations up to 1 nm, as perfectly flat graphene is thermodynamically unstable.⁹⁻¹¹ Due to its linear energy dispersion and conical band structure, graphene absorbs $\sim 2.3\%$ of light and thus can even be visible by naked eye (Figure 1.1b).^{12,13} Finally, graphene is one of the most thermally conductive materials with reported thermal conductivity values of $1500\text{--}2500 \text{ Wm}^{-1}\text{K}^{-1}$.^{14,15}

The combination of these most prominent properties made graphene one of the most studied materials since it had been isolated in 2004.¹ Graphene offers rich fundamental physics as well as vast application opportunities, including field effect transistors, gas sensors, wearable electronics, water filtration, DNA sequencing, to name a few.¹⁶⁻²² Most far reaching promises relate to the exploitation of its "all in one package" unique electronic properties, mechanical robustness, atomic thinness and large surface-to-volume ratio.

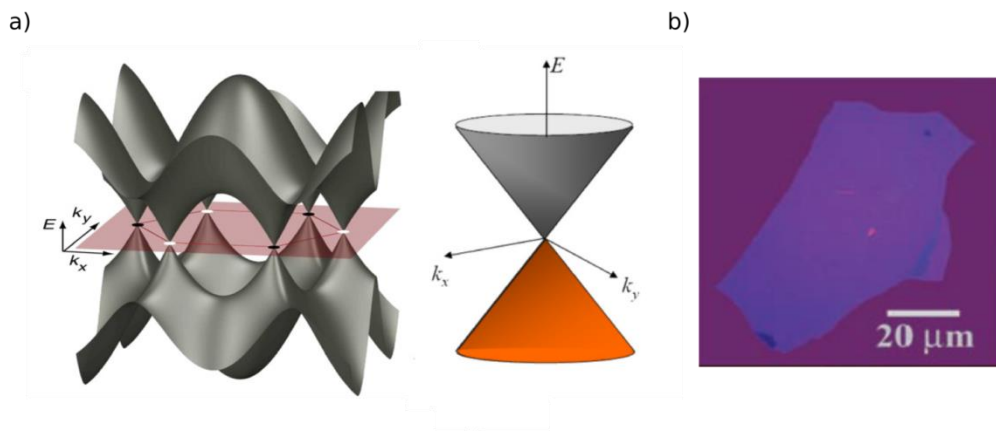


Figure 1.1. Electronic and optical properties of graphene. a) Dirac point and band structure of ideal monolayer graphene.²³ b) Optical image of a monolayer graphene flake exfoliated from graphite and transferred to a silicon/silicon oxide wafer (n-doped, with a silicon oxide layer of 300 nm) using the scotch tape method.¹

1.1. Fabrication of graphene

Mechanical exfoliation of graphite with scotch tape was the first successful method used to isolate a single layer of graphene (see Figure 1.1b for an example of mechanically-exfoliated monolayer graphene flake).¹ Although a great number of fundamental physical properties were discovered using mechanically-exfoliated graphene,^{7,24–27} the scotch-tape method only yields small micrometer-sized monolayer flakes with a very low yield (although of high quality). The expanding research and industrial interests demand – instead – larger flakes and scalable processes for producing graphene. Since 2004, various graphene production methods have been developed: chemical vapor deposition (CVD),^{28–34} chemical exfoliation of graphite and graphite oxide,^{35–37} epitaxial growth,³⁸ total organic synthesis,^{39,40} liquid-phase exfoliation (sonication of graphite suspensions),⁴¹ pyrolysis⁴² and carbon nanotube slicing.^{43,44} Depending on the method, graphene is obtained in the form of continuous supported monolayers (CVD, epitaxial growth, carbon nanotube slicing), powders or suspensions (chemical and liquid-phase exfoliation, pyrolysis). Each of these production

methods yield graphene of various structural characteristics, such as number of layers, crystallinity, flake size, intrinsic roughness, presence of functional groups, adatoms and defects.^{45,46} Such diversification, on one hand, creates a versatile toolbox for the usage of graphene, but, on the other hand, results in graphene materials with appreciably different (electronic and mechanical) characteristics and overall performance in devices, which must be considered whenever the generic “graphene” term occurs.⁴⁶

Currently, CVD proved to be the most optimal method to fabricate graphene on a large scale.^{28–34} Essentially, graphene is produced through the dehydrogenation of a hydrocarbon precursor (usually methane or ethene) in presence of a metal catalyst, followed by the adsorption of carbon atoms on the surface of the catalyst, which in a last step arrange into the hexagonal graphene lattice (Figure 1.2a). Typically, the growth process is self-limited, and terminates when the catalyst is passivated with a continuous graphene monolayer.⁴⁷ In some cases, however, single islands of bi- and few-layers graphene may grow (Figure 1.2b),⁴⁸ particularly on a metal such as nickel in which the solubility of carbon is higher, compare to copper.³³ Depending on the exact growth conditions, CVD can yield mono- or polycrystalline graphene with, in principle, controllable domain size and orientation,⁴⁹ and with charge carrier mobilities almost as high as in mechanically exfoliated graphene.^{50,51} Advantageously to other production methods, the maximal size of the graphene sheet is only limited by the dimensions of the oven, reportedly reaching $5 \times 50 \text{ cm}^2$.⁴⁹

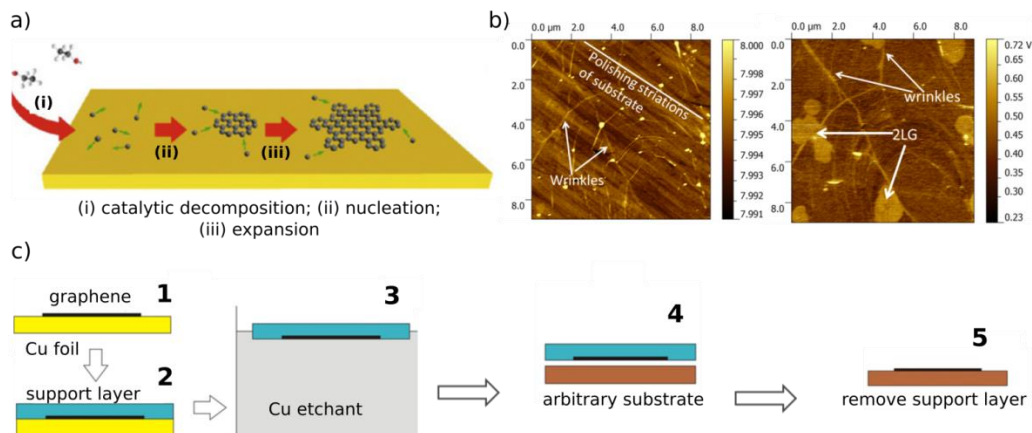


Figure 1.2. Most common methods to produce and transfer graphene on a large scale.

a) Illustration of chemical vapour deposition (CVD) for the growth of graphene on a metal catalyst.⁵² b) Atomic force microscopy (AFM) and scanning Kelvin probe microscopy (SKPM) images of CVD-grown graphene on a quartz substrate illustrating imperfections in graphene morphology common for CVD-grown samples: wrinkles, bilayers, grain boundaries.⁵³ c) Schematics of the most commonly used polymer-assisted method to transfer graphene:⁵⁴ 1) graphene is grown on copper, 2) a support polymeric layer is deposited on graphene on copper, 3) copper is etched, 4) the polymer/graphene stack is transferred on a target substrate, and 5) the polymer support layer is removed.

1.2. Methods to transfer graphene

The CVD method produces graphene on metallic (*i.e.* conductive) supports, while for most applications, especially in electrical circuits, an insulating layer underneath graphene is required. The routine transfer of an atomically thin layer from substrate to substrate, preserving the pristine excellent properties, is very challenging and stimulated the development of several transfer approaches. The earliest and the most common transfer method utilizes a polymer, typically poly(methyl methacrylate) (PMMA), as a support layer to preserve the integrity of graphene during the transfer (Figure 1.2c).^{54–57} After coating graphene with the polymer, the metal/graphene/polymer stack is placed floating on the surface of an aqueous solution of the metal etchant (Figure 1.2c). Then, once the metal support is fully etched, the graphene/polymer stack is transferred on the target

substrate (Figure 1.2c). In a last step, the polymer layer is dissolved in an organic solvent, typically acetone (Figure 1.2c). The use of a polymer support allows transferring large (centimeter-size) graphene sheets. The drawback, however, is that the polymer drastically contaminates the graphene surface,^{58,59} hindering its intrinsic thermal conductivity⁶⁰ and reducing charge carrier mobilities due to introduced doping and additional scattering sites.^{61–64} Moreover, polymer supports also induce extrinsic roughness and other morphological defects in graphene, affecting its properties.⁶⁵ Many potential applications of graphene are based on the exceptional sensitivity of its surface to the environment²⁰ and, therefore, transferring graphene using a clean transfer methodology is crucial.

To overcome the contamination introduced by polymers, several polymer-free strategies were developed.^{66–71} Generally, the transfer scheme resembles that of the polymer-assisted method, with the distinction that the polymer is substituted with a non-polymeric supporting layer, such as a metal,⁷² a naphthalene film,⁷¹ liquid hexane,⁶⁷ or even using graphite holders.⁶⁶ The major drawbacks of all polymer-free methods, however, are the morphological distortion of the graphene surface (cracks, wrinkles, folds) caused by the capillary forces and conformational mismatch between graphene and the supportive layer, which not only prevent the scalability of the transfer methods, but also alter the electronic, mechanical, thermal and wetting properties of graphene.^{65,73}

In summary, despite active research efforts, the transfer and handling of graphene still pose nontrivial challenges on the way towards widespread application and production of graphene-based devices. For the physics community exfoliated graphene still represents the standard, particularly since the discovery of the so called van der Waals heterostructures.⁷⁴ For larger graphene flakes, CVD graphene requires clean transfer methods. In Chapter 2 a new polymer-free transfer method is presented, which principally improved the quality of transferred graphene. In this method, the physical properties of cyclohexane were exploited to provide a soft and adaptable yet non-contaminating support to transfer centimeter-sized graphene layers. The electrical characterization of graphene at the water/cyclohexane interface confirmed the superior cleanness and charge carrier mobilities of the graphene which were compared to other well established transfer techniques.

1.3. Graphene at liquid interfaces

Graphene is atomically thin and, therefore, all the carbon atoms composing its surface are always in direct contact with the environment in which graphene is embedded. More precisely, each atom of graphene is always in contact with two media, the one at the bottom and the one on top of the graphene layer. The medium on one side of the graphene surface alters the work function (*i.e.* chemical potential) of graphene, which, in turn, affects the interactions between graphene and the medium on the other side. As a result, experimentally observed (electronic and chemical) properties of graphene are dictated not only by the electronic structure of graphene itself, but also by the combined effects of the interactions between graphene and the media from both sides. Furthermore, the interactions of any particular medium (solid surface, liquid, gas, molecules of adsorbate, etc.) with graphene must be interpreted in the context of the effect of the medium from the other side of graphene. For applications and research purposes where graphene cannot be free-standing in vacuum, understanding the interfacial physics and chemistry of graphene (especially CVD graphene) is, therefore, of paramount importance. Studying the physical and chemical phenomena at graphene interfaces, however, poses two main challenges: the uncontrollable alteration of the surface/physical/chemical properties of graphene introduced during transfer and handling, and the disentanglement of the intrinsic properties of graphene from the effects of the substrate and of the environment (even provided there are no transfer-related alterations).

Specifically, research focused on understanding the effect of the substrate on the properties of graphene. Strain and doping induced by the underlying substrate were found to play the most important roles in affecting the electronic band structure and phononic properties of graphene (Figure 1.3).^{75–81} In fact, unintentional non-uniform strain inevitably occurs due to the corrugations of the graphene sheet caused by the mismatch in structure^{79,81} and thermal expansion coefficients^{83,84} between the graphene and the substrate. Additionally, doping by the substrate is also ubiquitously present in supported graphene.^{80,85}

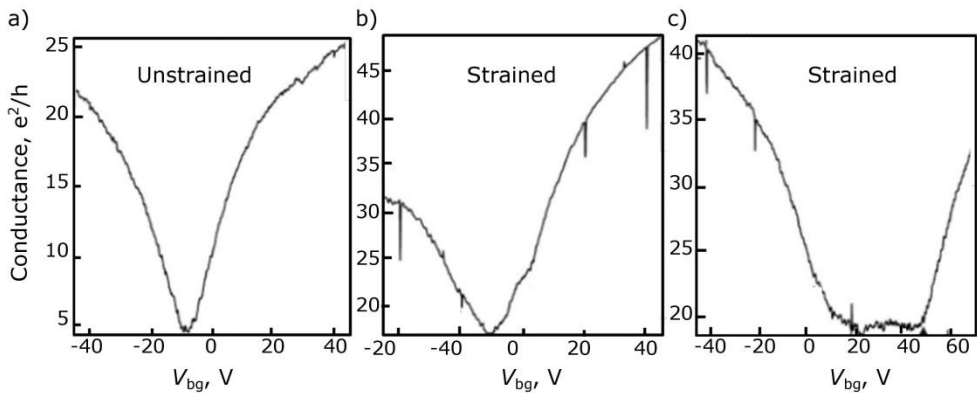


Figure 1.3. Effect of strain on the electronic properties of graphene. Gate voltage (V_{bg}) dependent sheet conductance measured at $T=1.5$ K and $V=100$ μ V for a) unstrained graphene and b, c) for graphene under applied uniaxial strain of different magnitudes.⁸¹

In contrast to graphene on solid supports, studies of graphene's behavior at liquid interfaces are scarce, and mostly limited to studies of the wettability of graphene on solid substrates (*i.e.* graphene at solid/liquid interfaces).⁸⁶ In Chapter 2 the properties of graphene at liquid/liquid interfaces were probed for the first time by measuring charge carrier mobilities of graphene free-floating directly at a liquid/liquid interface. A significant enhancement of the mobilities compared to graphene supported by conventional solid supports was observed at a water/cyclohexane interface. Next, in Chapter 3 confocal Raman spectroscopy was used to characterize graphene at liquid/air and liquid/liquid interfaces. It is shown that, in stark contrast to solid supports, liquid supports induce very small to zero strain and doping in graphene, which is in excellent agreement with the enhanced charge carrier mobilities reported in Chapter 2. Additionally, Chapter 3 exemplifies how the strain relaxation induced by liquid supports could be used to monitor hydrogenation or other functionalization of graphene.

Furthermore, Chapters 4, 5 and 6 present new insights and strategies for studying the wettability of supported, free-standing and free-floating graphene in water. Specifically, Chapter 4 reports the contact angle of fully free-standing graphene in air, Chapter 5 studies the wettability of graphene in water, particularly the diverse factors affecting the wetting of supported graphene, and Chapter 6 compares the interactions between graphene and water at a molecular and bulk levels.

1.4. Wettability of graphene.

The wettability of a solid surface characterizes its affinity to water and provides an indication about possible interactions with molecules other than water.^{87,88} For graphene, however, a simple measurement of the water contact angle yielded a remarkably wide range of values – from hydrophilic to hydrophobic^{89–92} – and an extensive debate over the origin of the contact angle discrepancies, which still seems not resolved. Most researchers now agree that, due to the atomic thickness of graphene, the underlying substrate has a critical effect on the apparent wettability of graphene.^{91,93–97} On the other hand, the extent to which graphene is transparent to wetting is still debated – graphene has been reported to be fully wetting transparent,⁹³ partially wetting transparent^{96,98,99} and fully opaque.^{91,92,100} As discussed previously, the apparent (*i.e.* observed experimentally) wettability of graphene is determined by the intrinsic wettability of graphene and external factors. The intrinsic wettability of graphene is dictated solely by the properties of pristine and isolated graphene, a situation which does not occur practically. All external factors altering the intrinsic wettability of graphene can be categorized into 1) fundamental substrate effects and 2) environmental effects. The substrate effects include well-defined (as opposed to environmental) effects of the polarity¹⁰¹ and doping of the substrate.^{102,103} In principle, the intrinsic wettability and the substrate effects are sufficient to describe the wettability of supported graphene. They are, however, often hindered by the environmental effects, which are induced unintentionally during sample preparation (different graphene production methods,^{104,105} transfer and handling-related contamination and structural irregularities⁵⁷) and measurement conditions (adsorption of air contaminants^{98,106}). Environmental factors do not represent the properties of graphene, nor of the substrate, and often cause non-negligible sample-to-sample variations and, therefore, must be minimized.¹⁰⁶ In practice, however, the contributions of the substrate and of the environment are difficult to disentangle. The following subchapters will introduce the intrinsic wettability of graphene, and discuss how it is affected by the substrate and the environment.

In addition to the conventional characterization of wettability in ambient by means of contact angle measurements, interactions between graphene and other molecules in ultra-high vacuum (UHV) were also investigated using surface science methods.^{107–113} For example, the comparison between the UHV and the ambient studies demonstrated that microscopic hydrophobicity does not straightforwardly translate into macroscopic hydrophobicity, but rather provides complementary insights.

1.4.1. Thermodynamics of graphene wetting

The surface energy of a solid σ_S is the interfacial tension of solid-gas interface σ_{SG} and is defined as an excess energy of its surface compared to the bulk, and related to the contact angle θ with the Young equation (Figure 1.4a):

$$\sigma_{SG} - \sigma_{SL} - \sigma_{LG} \cos\theta = 0,$$

where σ_{SL} is solid-liquid interfacial energy and σ_{LG} is liquid-gas interfacial energy (or surface tension of the liquid σ_L).

Graphene and other two-dimensional (2D) materials do not have a bulk phase, and, therefore, the definition of the surface energy cannot be applied to describe a completely isolated monolayer graphene. The contact angle and the surface energy of graphene, therefore, must be always regarded in the context of the underlying substrate (or liquid and gaseous medium underneath graphene). In fact, similarly to the water contact angle measurements, attempts to determine the surface energy of graphene resulted in very sparse and spreaded values. As a few examples, the surface energy was reported to be 46.7 mJ/m² for graphene on a silicon substrate (chemically exfoliated flakes),¹¹⁴ 62.2 ± 3.1 mJ/m² for graphene on copper (CVD),⁹⁸ 40.4 mJ/m² for graphene on PDMS (CVD),⁹⁶ 48.8 mJ/m² for graphene on glass⁹⁶ and 115±4 mJ/m² for suspended graphene (CVD).¹¹⁵ These examples demonstrate that the deviations from the structurally ideal non-contaminated graphene surface, caused by the environmental (production method, transfer, environment) factors and by the effect of the underlying substrate, result in graphene interfaces with significantly different

wetting properties. Theoretical studies also show disagreement: molecular dynamic (MD) simulations predict a surface energy of zero,¹¹⁶ whereas quantum Monte Carlo and advanced density-functional first-principles calculations predict values in the range 144-171 mJ/m².^{117,118} The type of interactions between graphene and a wetting liquid can be determined from the contributions of polar (hydrogen bonding, dipole-dipole and dipole-induced dipole) and dispersive (London-van der Waals) interactions to the total surface energy,¹¹⁹ by measuring multiple contact angle measurements with liquids of different polarities as described in Fowkes,¹²⁰ Owens-Wendt¹²¹ or Neumann model (Figure 1.4b).¹²²⁻¹²⁴ Interestingly, such an approach yielded more consistent results than determining the total surface energy (*i.e.* the sum of dispersive and polar contributions): most studies agree, in qualitative terms, on the dominance of the dispersion forces in the surface energy of graphene.^{96,98,101,125} Moreover, by comparing polar (σ_s^P) and dispersive (σ_s^D) components of graphene-on-a-substrate ($\sigma_{s_2}^D$ and $\sigma_{s_2}^P$ in Figure 1.4c) and those of the bare substrate ($\sigma_{s_1}^D$ and $\sigma_{s_1}^P$ in Figure 1.4c), the transmittance of graphene to specific interactions (polar or dispersive) can be estimated (Figure 1.4c),¹²⁶ providing new insights into the chemical origin of the wetting transparency of graphene.

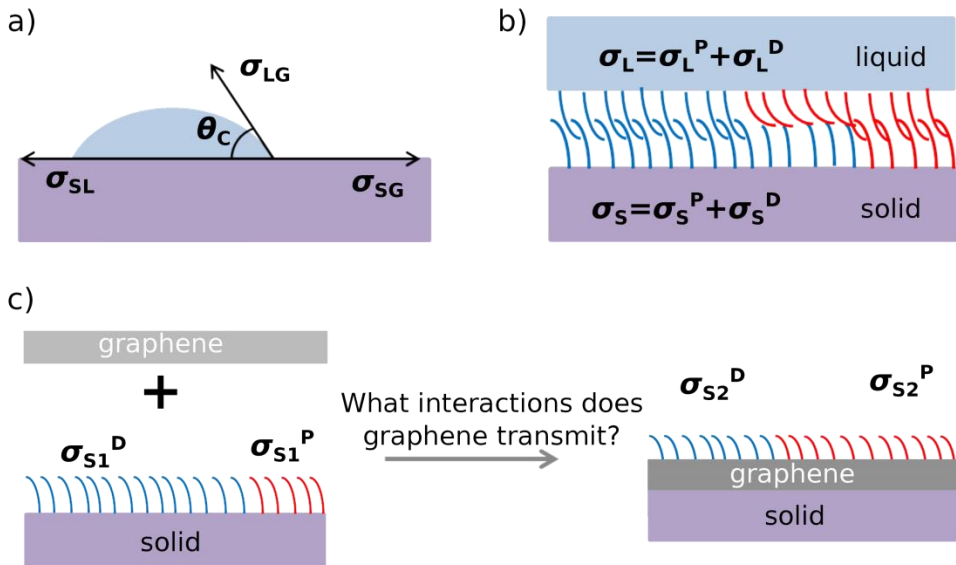


Figure 1.4. Thermodynamics of graphene wetting. a) Three phase equilibrium diagram in the sessile drop technique: θ_c is the contact angle and σ_{SL} , σ_{LG} and σ_{SG} are the interfacial tensions at solid-liquid, liquid-gas and solid-gas interfaces respectively. b) Model of polar and dispersive interactions between a solid and a liquid represented by the polar (σ_S^P and σ_L^P) and dispersive (σ_S^D and σ_L^D) components of the surface tensions σ_S and σ_L . Blue and red lines depict the contributions of dispersive and polar interactions respectively. c) Illustration of the effect of graphene transmitting polar and dispersive components of the surface energy of the solid substrate. The addition of a graphene layer on top of the solid changes the contributions of polar and dispersive interactions from σ_{S1}^D and σ_{S1}^P to σ_{S2}^D and σ_{S2}^P .

Chapter 5 demonstrates that in the case of a clean non-corrugated graphene-substrate interface (*i.e.* when the interface was not exposed to air and was not subjected to any transfer-related contamination and mechanical deformation), the graphene is transparent to both polar and dispersive interactions independently of the polarity of the substrate. Remarkably, graphene was almost entirely opaque to polar interactions when it was transferred on a substrate using PMMA transfer, presumably due to contamination and morphological distortions.

1.4.2. Wetting of free-standing graphene

The characterization of the intrinsic wetting properties of graphene is technically complicated, because both the environmental factors and the substrate contribute to the observed wetting characteristics. The influence of the substrate can be eliminated in a free-standing geometry. However, so far, it was only possible to make graphene free-standing over a few square micrometers, rendering difficult to measure the contact angle of a microliter droplet (with a millimeter range diameter). Simulations of the contact angle of water on free-standing graphene have been challenging as well and were shown to highly depend on the choice of the graphene-water interaction model. Suchwise, independent MD simulations resulted in the contact angles of suspended graphene as different as $90\text{-}127^\circ$ ^{91,127,128} and $45.7^\circ \pm 1.3^\circ$.¹²⁹

Only a few experimental approaches attempting to circumvent the complications of the conventional contact angle measurements yielded information on the intrinsic wettability of suspended graphene.^{73,90} In the first study, graphene was suspended over hydrophilic and hydrophobic nanopatterned silicon substrates (Figure 1.5a) with varying area fractions of suspended graphene. By extrapolation of the contact angle values of partially suspended graphene, the water contact angle for fully suspended graphene was estimated to be $85^\circ \pm 5^\circ$. Interestingly, the contact angle of partially suspended graphene did not depend on the area of suspended graphene (*i.e.* it was $85^\circ \pm 5^\circ$ for all measured area fractions, Figure 1.5b), and neither on the wettability of the underlying substrate (Figure 1.5b).⁷³ The major drawback of using partially suspended graphene, however, is that the deposition of monolayer graphene on such sharply patterned structures (the conical pillars were 5-15 nm in width, spaced by 10 nm, Figure 1.5a) and the water-based transfer method that was used, created a large density of wrinkles, pinholes and cracks which certainly alter the structural properties of the graphene surface.⁷³ Moreover, the ability of such suspended graphene structures to sustain the weight of a water droplet, particularly for contact angle measurement, was not supported experimentally and is, therefore, questionable.

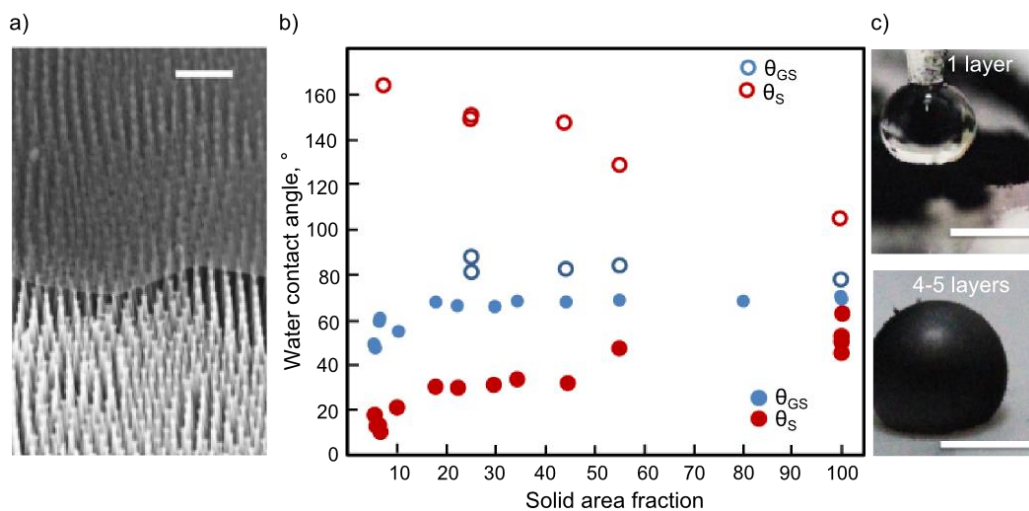


Figure 1.5. Experimental water contact angle measurements on free-standing graphene.

a) Scanning Electron microscopy (SEM) image of a graphene monolayer partially suspended over nanopatterned silicon pillars.⁷³ The scale bar represents 200 nm. b) Contact angle as a function of solid area fraction at the top of the texture.⁷³: water contact angle values for bare hydrophilic pillars (θ_s) are represented by filled red circles, for bare hydrophobic pillars – by hollow red circles; water contact angle values for graphene deposited on hydrophobic and hydrophilic substrates (θ_{GS}) are represented by hollow and filled blue circles respectively. c) Graphene (reduced graphene oxide) nanopowders of monolayer (top) and 4-5 layers (bottom) flakes in contact with a water droplet, *i.e.* the “liquid marble” experiment.⁹⁰ The scale bars represent 2 mm.

In a second study, the wetting properties of suspended graphene were characterized based on the ability of graphene nanopowders to adsorb water.⁹⁰ Graphene nanopowders consisted of nanoflakes of reduced graphene oxide separated by air cavities and, therefore, represented free-standing graphene. Remarkably, water adsorption measurements on such graphene nanopowders of different thicknesses (*i.e.* flakes with different number of stacked graphene monolayers) yielded contact angles of $179^\circ \pm 2^\circ$ (for nanopowders with monolayer flakes), $163^\circ \pm 2^\circ$ (for nanopowders with the flakes of 4-5 layers) and $140^\circ \pm 2^\circ$ (for nanopowders with the flakes of 25 layers).⁹⁰ The “liquid marbles” experiments, in which the ability of a powder to adsorb on a water droplet is tested, also showed

that the nanopowder composed of monolayer flakes is superhydrophobic (no flakes adsorbed on the surface of the droplet, Figure 1.5c) while nanopowder samples with 4-5 layers flakes showed a hydrophobic character (the flakes indeed adsorbed on the surface of the droplet, without intruding inside the droplet, Figure 1.5c). Although the experimental approach was clever from a methodological point of view, reduced graphene oxide powders are, however, different from pristine graphene monolayer as they are structurally disordered materials containing significant amount of oxidized edges (based on Raman spectroscopy and chemical analysis) particularly the powder containing the thinnest flakes (~one layer).

In addition, besides still being indirect indications of the wettability of free-standing graphene, the two approaches described above do not take into account the adsorption of airborne hydrocarbons which are known to substantially alter wetting of graphitic surfaces.^{129,130}

In Chapter 4 a direct contact angle measurement on fully free-standing graphene in air was realized using the so-called captive bubble method, which avoids the mechanical tearing of graphene because of the droplet weight. The captive bubble approach also prevents handling-related structural deformations and contamination of graphene, and, importantly, airborne hydrocarbons adsorption. Essentially, in the captive bubble method an air bubble is injected underneath a graphene monolayer floating at the water-air interface, intrinsically forming a millimeter-scale air-suspended graphene, allowing for the direct measurement of the contact angle, and hence the wettability of free-standing graphene. In contrast with the studies on partially suspended graphene and nanopowders of reduced graphene oxide, the captive bubble method showed that graphene is hydrophilic with a measured water contact angle of $42^\circ \pm 3^\circ$. Distinctively, the captive bubble experimental design provides measurements on large area of smooth (*i.e.* graphene floats on the surface of water) fully free-standing graphene avoiding any transfer-related contamination and adsorption of hydrocarbons.¹⁰⁶

1.4.3. Effects of the substrate on the wettability of graphene

The substrate on which graphene is transferred or grown has a strong influence on the wettability of graphene. In fact, the underlying substrate alters the electronic structure and, consequently, the chemical potential of graphene. The first MD modelling of van der Waals (vdW) interactions between a liquid and a graphene sheet introduced the “wetting translucency” as opposed to the “wetting transparency” of graphene and suggested that wetting transparency does not occur when graphene is supported by superhydrophobic or superhydrophilic substrates.⁹⁵ The model, however, assumes that the solid-liquid interactions are dominated by vdW forces and does not take into account the electrostatic interactions or hydrogen bonding between liquids and solids, which could also contribute to the wetting properties.

Interestingly, density-functional theory (DFT) calculations showed that the dipole moment of water does not affect the electronic structure and doping in fully suspended graphene.^{89,132} However, if a solid substrate is present (namely, SiO₂¹³² and copper¹⁰¹), the subsequent charge transfer between the substrate and the graphene triggers the polarization effect of water on graphene¹³² and modulates the Fermi level of graphene,^{101,133} all of which result in altering the graphene-water interactions and, therefore, the apparent macroscopic wettability.

Finally, experimental studies also confirmed that inducing p- or n-doping by applying a gate voltage (Figure 1.6a),¹⁰² or by introducing a layer of metal or polyelectrolytes (namely poly(sodium 4-styrenesulfonate), poly(acrylic acid), poly(allylamine hydrochloride) and poly-L-lysine) between graphene and the substrate, and by fabricating metal-graphene heterojunctions,¹⁰³ alters the properties of graphene towards more hydrophilic (Figure 1.6b).^{102,103} According to DFT and molecular dynamics calculations, the induced doping modulates the charge carrier density in graphene and binding energy between graphene and water, which affects the wettability of graphene.¹⁰³

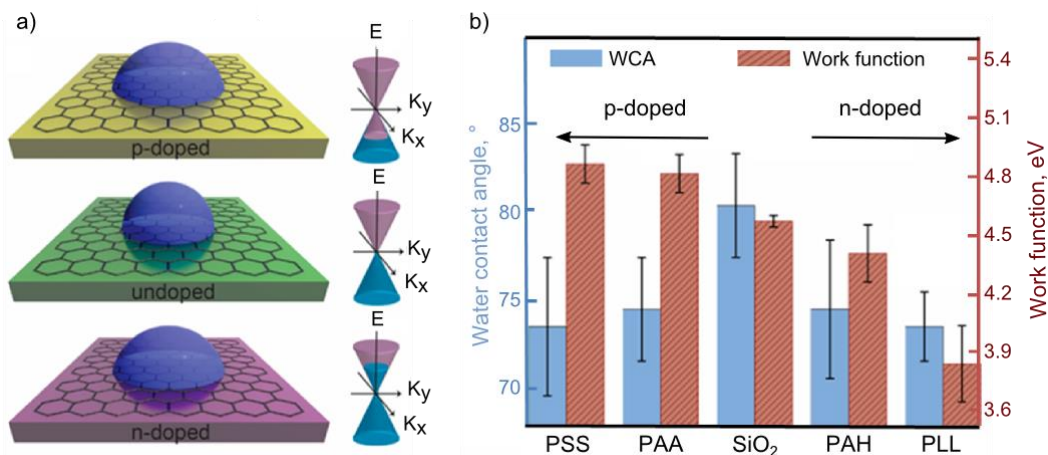


Figure 1.6. Effect of doping on the water contact angle of graphene. a) Illustration of the effect of the doping-induced shift of the Fermi level of graphene on the measured water contact angle.¹⁰³ b) Water contact angle and work function of undoped graphene on SiO₂ substrate and of graphene doped by introducing a layer of poly(sodium 4-styrenesulfonate) (PSS), poly(acrylic acid) (PAA), poly(allylamine hydrochloride) (PAH) and poly-L-lysine (PLL) between graphene and the SiO₂ substrate.¹⁰³

1.4.4. Environmental factors affecting the wettability of graphene

Environmental factors are the factors responsible for the variability of reported contact angles due to sample preparation and measurement conditions (adsorption of airborne hydrocarbons, growth and transfer of graphene).

The adsorption of airborne hydrocarbons is the major cause of the false apparent hydrophobicity of graphitic surfaces and false apparent contact angle of $\sim 90^\circ$.^{106,129,133–136} In fact, ellipsometry and attenuated total reflectance-Fourier transform infrared spectroscopy (ATR-FTIR) studies showed that a 5 Å thick layer of hydrocarbon contaminants forms on graphite upon exposure to air.¹³⁸ Disproving the long-held belief, first, graphite,¹³⁰ and then graphene^{98,106} were demonstrated to be intrinsically mildly hydrophilic exhibiting contact angles of $\sim 60^\circ$ and $\sim 40^\circ$ (for graphene on copper) respectively, when the measurements were conducted on contamination-free samples (Figure 1.7a). Hydrocarbons are

ubiquitously present in the environment. Even storing graphene samples in a plastic Petri dish as opposed to a glass one results in a noticeable increase of the contact angle in the course of fifteen minutes (Figure 1.7b).¹⁰⁶ Thermal annealing, ultraviolet ozone treatment¹⁰⁶ and hydrogen plasma¹³⁹ can be utilized to remove the adsorbed hydrocarbons from graphene (Figure 1.7c). Another way to preserve the intrinsic wettability of graphene is to store graphene at low temperature (-15°C): a protective layer of ice forms on the graphene surface preventing hydrocarbon adsorption.¹⁴⁰ Contact angle measurements (and any other surface inspection) on graphene samples must, therefore, be conducted within minutes after growth or using the surface treatments mentioned above.

Separately, the broad diversity of synthetic¹⁰⁴ and transfer⁵⁷ methods yield graphene materials with different surface properties.^{45,105} Most wettability studies were performed on CVD grown graphene, as CVD is the most convenient method to produce large sheets of monolayer graphene up to now, suitable for contact angle measurements.²⁸⁻³⁴ However, even considering only CVD graphene samples, varying the growth conditions (catalytic metal, morphology of the substrate, temperature, pressure, annealing conditions, precursor gas, gas flow, presence of oxygen and hydrogen) results in different number of layers, domain size and orientation, type and density of defects, density of oxidized carbon atoms, size and density of wrinkles and other morphological features, which affect the wetting behavior of graphene.¹⁴¹ For example, the introduction of point defects in the graphene lattice using an oxygen plasma changed the contact angle of graphene on SiC from 92.5° to 55.1°, and the subsequent restoration of the graphene lattice upon annealing in UHV increased the contact angle to 87.3°, close to the pristine value.¹⁰⁰ Separately, the effect of line defects (dislocations and grain boundaries) on the wetting of graphene was probed by scanning tunnelling microscopy (STM) and indicated that interactions between water and line defects in graphene caused water to intercalate and split the graphene into fragments.¹⁴² Interestingly, this phenomenon was shown to be substrate-dependent and was observed for graphene on Ru(0001) but not on Cu(111), with copper known to interact more weakly with graphene.¹⁴² Also, a number of MD studies reported that the imperfections in graphene, such as multilayers,¹²⁶ holes¹⁴³ and roughness^{99,126} generate a variety of wetting states (Figure 1.7d),

naturally implying that varying their concentrations and dimensions would result in different wettabilities.

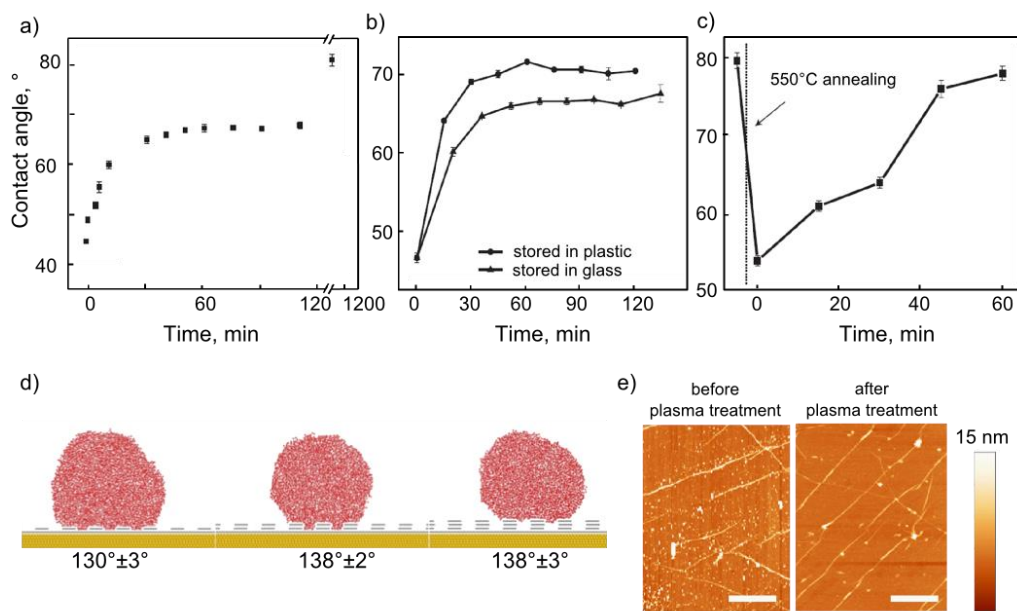


Figure 1.7. Environmental effects affecting the wettability of graphene. a) Water contact angle of monolayer graphene-on-copper upon exposure to ambient air after CVD growth.¹⁰⁶ b) Water contact angles of graphene-on-copper stored in plastic and glass Petri dishes as a function of storage time.¹⁰⁶ c) Effect of annealing at 550°C in argon atmosphere on the water contact angle of graphene on copper.¹⁰⁶ d) MD simulation of the effect of surface morphology on the water contact angle of graphene.¹²⁶ e) AFM images of wrinkles, folds, contamination and other imperfections in graphene transferred on a Si/SiO₂ substrate using the PMMA-assisted method before (left) and after (right) hydrogen plasma.¹³⁹

Yet, the transfer of graphene from the growth catalyst to a target substrate induces even larger irregularities (ripples, folds, cracks, contamination) in the graphene structure and graphene-substrate interface, and causes additional sample-to-sample variations (Figure 1.7e).^{62,138,144} The most widely used polymer-based transfer methods irreversibly contaminate the surface with polymer residues (Figure 1.7e),^{144,146–148} whereas alternative polymer-free transfer

methods provide minimal contamination,^{66–70} but often at the cost of disintegrity and formation of micrometer-sized folds and wrinkles in the graphene layer.⁶⁴

Chapter 5 presents a comparative study of three types of samples: non-transferred graphene samples, graphene transferred using a polymer-free method and samples transferred using PMMA. Interestingly, non-transferred graphene samples were transparent to wetting, graphene transferred using a polymer-free method significantly altered the contact angle and surface energy of the substrate, and samples transferred using PMMA yielded irreproducible wetting behavior, suggesting that transfer, contamination and handling yield graphene with large sample-to-sample variation from very hydrophilic to hydrophobic.

1.4.5. Microscopic wettability of graphene

In parallel with the macroscopic investigations in ambient atmosphere, surface science methods were also employed to probe the affinity of water molecules to graphene under UHV conditions, the so-called “microscopic wettability” or wettability at the molecular level.^{107–113,149–151} Measurements under UHV provide extreme pureness of the environment and sensitivity and can, in principle, allow the accurate probing of the interactions between graphene and single water molecules. Temperature programmed desorption (TPD) is a method typically used for investigating the microscopic wettability of surfaces.¹⁵² Essentially, a TPD experiment yields a desorption curve which represents the amount of water molecules (or of other adsorbate) desorbing from a surface upon heating. Typically, a set of curves is recorded at different initial partial pressures of water in the UHV chamber (that is, different coverages of the studied surface with water). The onset temperature at which molecules start desorbing, the shape of the curves and the evolution of the curves with increasing coverage (alignment of the leading edges, tails etc.) provide information about the desorption energy, the kinetic order of desorption, the binding energy and the ordering of the adsorbate molecules in the first and subsequent adsorbate layers.¹⁵²

It must be noted, however, that the wettability at the molecular level cannot be directly compared with the macroscopically observed wettability, as

experimental conditions are different (*i.e.* UHV versus ambient) and TPD studies refer to different molecular events (*i.e.* the adsorption of single molecules versus a collective adsorption of molecules in contact angle measurements). The difference between desorption and reaction mechanisms in UHV and ambient atmosphere, the so-called “pressure gap”, is an interesting subject on its own, and most recent advances in understanding its physical nature can be found elsewhere.¹⁵³

A number of thorough studies reported on the desorption kinetics of water,¹⁰⁹ methanol,¹⁰⁹ ethanol,¹⁰⁹ Ar,¹¹¹ Kr,¹¹¹ Xe,¹¹¹ N₂,¹¹¹ O₂,¹¹¹ CO,¹¹¹ methane,¹¹¹ ethane,¹¹¹ propane,¹¹¹ benzene¹¹² and cyclohexane¹¹² from graphene grown on Pt(111) *in situ* in a UHV chamber. Interestingly, while most adsorbates showed kinetic orders and desorption energies very similar to those on highly oriented pyrolytic graphite (HOPG),¹⁵⁴ water displayed a more complicated behavior at submonolayer coverages (*i.e.* when the amount of water molecules is not enough to form a continuous monolayer): misaligned leading edges, “dips” and “bumps”, peak shifts to higher temperatures upon desorption of the second and subsequent layers. It was reported that the first monolayer of water forms a new ice polymorph on graphene, in which planar hexagons of water molecules are stacked directly on top of each other, maximizing the number of hydrogen bonds (at the expense of their weakening), as opposed to normal puckered three dimensional (3D) hexagonal ice (Figure 1.8a).^{107,109} Although this phenomenon was previously predicted as a result of the confinement of water between two hydrophobic surfaces,^{155,156} the low energy electron diffraction, reflection–absorption infrared spectroscopy and rare-gas adsorption/desorption measurements showed that the surface of graphene actuates the unusual planar ordering of water molecules without any confinement. All other adsorbates (except benzene) manifested zero order kinetics desorption from graphene-on-platinum (111), indicating formation of the islands of condensed adsorbate in equilibrium with individual adsorbate molecules.^{109,111,157} In contrast, benzene showed a first order kinetics at submonolayer coverages on graphene-on-platinum (111), which transitions to zero order for the second and subsequent adsorbed layers, indicating that island formation (*i.e.* when the adsorbate forms multilayer islands instead of continuous monolayer) is unfavorable for aromatic molecules due to the weaker adsorbate-adsorbate (compared to adsorbate-

substrate) attractive interactions.¹¹² In that respect, benzene wets graphene on Pt(111) similarly to HOPG.¹⁵⁸ Methanol and ethanol, on one hand, have similar desorption energies on graphene and on HOPG, but on the other, presented a zero kinetic order on graphene, as opposed to the fractional kinetics orders on HOPG (0.26 and 0.08 respectively).^{109,159,160}

By comparing the desorption characteristics of graphene on various substrates with those of the bare substrates, the substrate effect and the wetting transparency were assessed.^{113,150,151} Interestingly, the transparency of graphene to desorption was shown to strongly depend on the adsorbate. Particularly, silicon and copper substrates strongly affect desorption of benzene,¹⁵⁰ n-pentane,¹¹³ butane¹⁵¹ and water¹⁴⁹ from graphene, even manifesting full transparency in the case of benzene (no data was presented for the desorption of n-pentane and butane from bare substrates thus no conclusion about wetting transparency in these cases could be made). The effect of the substrate on the microscopic wettability of graphene can be deduced as a difference between desorption energies of an adsorbate from graphene-on-a-substrate and from the bare substrate.^{113,150,151} For example, the desorption energies and their coverage dependences of benzene on copper and on silicon were not affected by the graphene layer at all (Figure 1.8b and c).¹⁵⁰ Water, in contrast, exhibits different desorption characteristics (kinetic order and desorption energy) on substrates (namely, silicon and copper) with and without graphene layer.¹⁴⁹ Interestingly, graphene-coated SiO₂ appeared to be more hydrophilic than bare SiO₂, and graphene-coated copper appeared to be more hydrophobic than bare copper.¹⁴⁹ Also, a complex desorption behavior of graphene on ruthenium (0001) was reported: no transparency to the desorption of water¹¹⁰ and benzene,¹⁰⁸ but full transparency to desorption of n-butane.¹⁵¹ These findings can be related to the fact that water intercalates and splits graphene on Ru(0001), as it was observed by STM.¹⁴²

Finally, the preparation and the quality of graphene samples must be taken into consideration in microscopic wettability studies as it is in the macroscopic contact angle measurements. In fact, graphene on Pt(111) and Ru(0001) were grown *in situ* in the UHV chamber, graphene on copper was grown using the CVD method and then mounted in the UHV chamber for desorption measurements, and graphene on SiO₂ was grown by CVD and then transferred using the PMMA-

assisted method (with polymer residues inevitably adsorbed on the graphene surface). Certainly, graphene grown *in situ* in UHV on well-defined smooth and extremely clean metallic surfaces is expected to be of higher quality and to represent properties of a single layer of ideal (non-contaminated and free of bulk defects) graphene. Such samples, however, are only relevant to fundamental UHV studies, and there are no available contact angles for a comparative analysis. Samples which were exposed to air and underwent a transfer step (graphene on copper and SiO₂), on the other hand, are widely used and studied, but have structural defects and contamination, especially for graphene on SiO₂.

Overall, surface science methods allow probing the interactions between graphene and individual molecules in ultra-pure environment and determination of the energy of desorption (which characterizes the strength of the interactions) and kinetic order of desorption (indicates how the molecules pack on the graphene surface). However, correlating the interaction parameters of individual molecules in UHV with the macroscopic wettability of graphene in ambient atmosphere is not straightforward. As well as in the case of macroscopic measurements, inconsistencies associated with the sample preparation pose a real challenge for the interpretation and the comparison between different sets of data, especially between microscopic (samples are prepared in UHV) and macroscopic (samples are exposed to air) studies. A systematic comparative analysis, which takes into consideration the effect of the sample preparation, is, therefore, needed.

In order to bridge the gap between the macroscopic and microscopic approaches, in Chapter 6 a comparative study was conducted on the effect of the irregularities in the graphene surface introduced during the transfer of graphene with the wettability both at a microscopic (water desorption measurements under UHV) and at the macroscopic level (contact angle measurements). Testing exactly the same samples in both TPD and contact angle measurements ensured the possibility to systematically compare the two approaches. Interestingly, the transparency of graphene to macroscopic wetting does not necessarily translate into the transparency to desorption of individual water molecules. While variations in roughness of the substrate seem to be of primary importance for the interactions between graphene and individual water molecules in vacuum, the

macroscopic wettability of graphene, in contrast, depends more strongly on the chemical composition of the substrate.

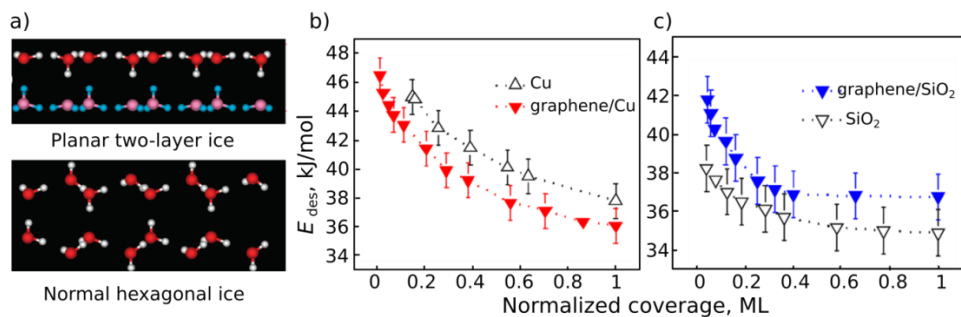


Figure 1.8. Molecular adsorption on graphene or microscopic wettability of graphene under UHV. a) Calculated structures (side view) of the planar two-layers polymorph of water ice that forms on graphene (top) and normal three-dimensional hexagonal water ice (bottom).¹⁰⁷ b) Desorption energy (E_{des}) as a function of benzene coverage (with ML depicting the number of benzene monolayers desorbed from the surface) for desorption of benzene from bare copper and graphene-on-copper.¹⁵⁰ c) Desorption energy (E_{des}) as a function of benzene coverage (ML – number of benzene monolayers desorbed from the surface) for desorption of benzene from bare SiO₂ and graphene-on-SiO₂.¹⁵⁰

1.5. Aim and outline

In this thesis unconventional tools based on fluidic interfaces were developed to study the surface and interfacial chemistry of graphene, to characterize the intrinsic properties of graphene, to disentangle the effects of substrate and of the environmental factors, and to improve handling protocols towards the preservation of the graphene cleanliness, morphology and electrical properties.

In Chapter 2 a liquid biphasic system was developed to transfer graphene without using a polymer support. Additionally, by probing electrically graphene *in situ* at a water/cyclohexane interface, an enhancement of charge carrier mobilities compared to supported graphene was observed, which was the first indication of the benefit of using a liquid interface to preserve the properties of pristine graphene.

Chapter 3 demonstrates how confocal Raman spectroscopy can be used to study graphene at a liquid/air and liquid/liquid interface, and presented a correlation study of graphene Raman bands. The results demonstrated that, unlike solid substrates, liquids do not induce strain and doping in graphene and are ideal supports for preserving the intrinsic electronic properties of graphene.

Chapter 4 further exemplifies how a liquid support can be used to probe the wettability of free-standing graphene revealing that graphene is inherently mildly hydrophilic.

Chapter 5 introduces ice and hydrogels as alternative supports for studying graphene-water interactions. The results show that graphene is hydrophilic in water and fully transparent to water-water interactions. Additionally, the selective transmittance of polar and dispersive interactions through graphene layer was investigated. Interestingly, while being fully transparent to dispersive interactions, graphene screens polar interactions in the samples that underwent a transfer step, presumably due to the structural distortions in the graphene layer induced by the transfer.

Finally, in Chapter 6 the macroscopic wettability in ambient atmosphere and the microscopic wettability under UHV conditions were systematically compared. The analysis showed that, while providing insights into the fundamental parameters

of graphene-water interactions, the microscopic wettability cannot characterize the macroscopic wettability of graphene. Additionally, the roughness of the underlying substrate was shown to affect the microscopic wettability and wetting transparency of graphene in UHV.

The use of liquid interfaces in graphene research is now emerging, and this thesis shows that the structural adaptability, molecular smoothness and weaker (compared to solids) intermolecular bonding of fluidic interfaces allow for experimental designs radically different from those involving solid substrates. By demonstrating that fluidic interfaces preserve graphene clean, smooth, unstrained and undoped, and by exploiting these advantages, a step forward was made to the design of (more) accessible and efficient graphene-based devices and technologies.

1.6. References

1. K. S. Novoselov, S. V. Morozov, D. Jiang, Y. Zhang, S. V. Dubonos, I. V. Grigorieva, A. A. Firsov, A. K. G. Electric field effect in atomically thin carbon films. *Science* **306**, 666–669 (2004).
2. Castro Neto, A. H., Guinea, F., Peres, N. M. R., Novoselov, K. S. & Geim, A. K. The electronic properties of graphene. *Rev. Mod. Phys.* **81**, 109–162 (2009).
3. Jorio, A., Dresselhaus, G. & Dresselhaus, M. S. *Carbon nanotubes: advanced topics in the synthesis, structure, properties and applications*. (Springer Berlin Heidelberg, 2007).
4. Geim, A. K. & Novoselov, K. S. The rise of graphene. *Nat. Mater.* **6**, 183–191 (2007).
5. Novoselov, K. S. *et al.* Two-dimensional gas of massless Dirac fermions in graphene. *Nature* **438**, 197–200 (2005).
6. Gusynin, V. P. & Sharapov, S. G. Unconventional integer quantum Hall effect in graphene. *Phys. Rev. Lett.* **95**, 146801 (2005).
7. Novoselov, K. S. *et al.* Room-temperature quantum Hall effect in graphene. *Science* **315**, 1379–1379 (2007).
8. Lee, C., Wei, X., Kysar, J. W. & Hone, J. Measurement of the elastic properties and intrinsic strength of monolayer graphene. *Science* **321**, 385–388 (2008).
9. Meyer, J. C. *et al.* The structure of suspended graphene sheets. *Nature* **446**, 60–63 (2007).
10. Fasolino, A., Los, J. H. & Katsnelson, M. I. Intrinsic ripples in graphene. *Nat. Mater.* **6**, 858–861 (2007).
11. Carlsson, J. M. Buckle or break. *Nat. Mater.* **6**, 801–802 (2007).
12. Nair, R. R. *et al.* Fine structure constant defines visual transparency of graphene. *Science* **320**, 1308 (2008).
13. Kuzmenko, A. B., van Heumen, E., Carbone, F. & van der Marel, D. Universal optical conductance of graphite. *Phys. Rev. Lett.* **100**, 117401

(2008).

14. Faugeras, C. *et al.* Thermal conductivity of graphene in Corbino membrane geometry. *ACS Nano* **4**, 1889–1892 (2010).
15. Cai, W. *et al.* Thermal transport in suspended and supported monolayer graphene grown by chemical vapor deposition. *Nano Lett.* **10**, 1645–1651 (2010).
16. Seo, D. H. *et al.* Anti-fouling graphene-based membranes for effective water desalination. *Nat. Commun.* **9**, 683 (2018).
17. Singh, E., Meyyappan, M. & Nalwa, H. S. Flexible graphene-based wearable gas and chemical sensors. *ACS Appl. Mater. Interfaces* **9**, 34544–34586 (2017).
18. Lemme, M. C., Echtermeyer, T. J., Baus, M. & Kurz, H. A Graphene field-effect device. *IEEE Electron Device Lett.* **28**, 282–284 (2007).
19. Matyba, P., Yamaguchi, H., Eda, G., Chhowalla, M., Edman, L. y Robinson, N. D. Graphene and mobile ions: the key to all plastic, solution processed light emitting devices. *ACS Nano* **4**, 637–642 (2010).
20. Schedin, F. *et al.* Detection of individual gas molecules adsorbed on graphene. *Nat. Mater.* **6**, 652–655 (2007).
21. Arjmandi-Tash, H., Belyaeva, L. A. & Schneider, G. F. Single molecule detection with graphene and other two-dimensional materials: nanopores and beyond. *Chem. Soc. Rev.* **45**, 476–493 (2016).
22. Heerema, S. J. & Dekker, C. Graphene nanodevices for DNA sequencing. *Nat. Nanotechnol.* **11**, 127–136 (2016).
23. Du, E. Y. A. and G. L. and X. Electronic properties of graphene: a perspective from scanning tunneling microscopy and magnetotransport. *Reports Prog. Phys.* **75**, 56501 (2012).
24. Novoselov, K. S. *et al.* Two-dimensional gas of massless Dirac fermions in graphene. *Nature* **438**, 197–200 (2005).
25. Novoselov, K. S. *et al.* Unconventional quantum Hall effect and Berry's phase of 2π in bilayer graphene. *Nat. Phys.* **2**, 177–180 (2006).
26. Katsnelson, M. I., Novoselov, K. S. & Geim, A. K. Chiral tunnelling and the

- Klein paradox in graphene. *Nat. Phys.* **2**, 620–625 (2006).
27. Pisana, S. *et al.* Breakdown of the adiabatic Born–Oppenheimer approximation in graphene. *Nat. Mater.* **6**, 198–201 (2007).
 28. Yu, Q. *et al.* Graphene segregated on Ni surfaces and transferred to insulators. *Appl. Phys. Lett.* **93**, 113103 (2008).
 29. Arco, L. G. De, Zhang, Y., Kumar, A. & Zhou, C. Synthesis, transfer, and devices of single- and few-layer graphene by chemical vapor deposition. *IEEE Trans. Nanotechnol.* **8**, 135–138 (2009).
 30. Reina, A. *et al.* Large area, few-layer graphene films on arbitrary substrates by chemical vapor deposition. *Nano Lett.* **9**, 30–35 (2009).
 31. Kim, K. S. *et al.* Large-scale pattern growth of graphene films for stretchable transparent electrodes. *Nature* **457**, 706–710 (2009).
 32. Li, X. *et al.* Large-area synthesis of high-quality and uniform graphene films on copper foils. *Science* **324**, 1312–1314 (2009).
 33. Zhang, Y., Zhang, L. & Zhou, C. Review of chemical vapor deposition of graphene and related applications. *Acc. Chem. Res.* **46**, 2329–2339 (2013).
 34. Lee, H. C. *et al.* Synthesis of single-layer graphene: a review of recent development. *Procedia Chem.* **19**, 916–921 (2016).
 35. Chen, G., Wu, D., Weng, W. & Wu, C. Exfoliation of graphite flake and its nanocomposites. *Carbon N. Y.* **41**, 619–621 (2003).
 36. Dreyer, D. R., Park, S., Bielawski, C. W. & Ruoff, R. S. The chemistry of graphene oxide. *Chem. Soc. Rev.* **39**, 228–240 (2010).
 37. Zhan, D. *et al.* FeCl₃-based few-layer graphene intercalation compounds: single linear dispersion electronic band structure and strong charge transfer doping. *Adv. Funct. Mater.* **20**, 3504–3509 (2010).
 38. Emtsev, K. V. *et al.* Towards wafer-size graphene layers by atmospheric pressure graphitization of silicon carbide. *Nat. Mater.* **8**, 203–207 (2009).
 39. Dötz, F., Brand, J. D., Ito, S., Gherghel, L. & Müllen, K. Synthesis of large polycyclic aromatic hydrocarbons: variation of size and periphery. *J. Am. Chem. Soc.* **122**, 7707–7717 (2000).

40. Segawa, Y., Ito, H. & Itami, K. Structurally uniform and atomically precise carbon nanostructures. *Nat. Rev. Mater.* **1**, 15002 (2016).
41. Hernandez, Y. *et al.* High-yield production of graphene by liquid-phase exfoliation of graphite. *Nat. Nanotechnol.* **3**, 563–568 (2008).
42. Choucair, M., Thordarson, P. & Stride, J. A. Gram-scale production of graphene based on solvothermal synthesis and sonication. *Nat. Nanotechnol.* **4**, 30–33 (2008).
43. Jiao, L., Zhang, L., Wang, X., Diankov, G. & Dai, H. Narrow graphene nanoribbons from carbon nanotubes. *Nature* **458**, 877–880 (2009).
44. Kosynkin, D. V *et al.* Longitudinal unzipping of carbon nanotubes to form graphene nanoribbons. *Nature* **458**, 872–876 (2009).
45. Shams, S. S., Zhang, R. & Zhu, J. Graphene synthesis: A Review. *Mater. Sci.* **33**, 566–578 (2015).
46. Kauling, A. P. *et al.* The worldwide graphene flake production. *Adv. Mater.* **0**, 1803784 (2018).
47. Li, X. *et al.* Large area synthesis of high quality and uniform graphene films on copper foils. *Science* **324**, 1312–1314 (2009).
48. Robertson, A. W. & Warner, J. H. Hexagonal single crystal domains of few-layer graphene on copper foils. *Nano Lett.* **11**, 1182–1189 (2011).
49. Xu, X. *et al.* Ultrafast epitaxial growth of metre-sized single-crystal graphene on industrial Cu foil. *Sci. Bull.* **62**, 1074–1080 (2017).
50. Banszerus, L. *et al.* Ultrahigh-mobility graphene devices from chemical vapor deposition on reusable copper. *Sci. Adv.* **1**, e1500222 (2015).
51. Petrone, N. *et al.* Chemical vapor deposition-derived graphene with electrical performance of exfoliated graphene. *Nano Lett.* **12**, 2751–2756 (2012).
52. Chen, X., Zhang, L. & Chen, S. Large area CVD growth of graphene. *Synth. Met.* **210**, 95–108 (2015).
53. Wang, R. *et al.* Investigation of CVD graphene topography and surface electrical properties. *Surf. Topogr. Metrol. Prop.* **4**, 25001 (2016).

54. Suk, J. W. *et al.* Transfer of CVD-grown monolayer graphene onto arbitrary substrates. *ACS Nano* **5**, 6916–6924 (2011).
55. Li, X. *et al.* Transfer of large-area graphene films for high-performance transparent conductive electrodes. *Nano Lett.* **9**, 4359–4363 (2009).
56. Gao, L. *et al.* Face-to-face transfer of wafer-scale graphene films. *Nature* **505**, 190–194 (2013).
57. Chen, M., Haddon, R. C., Yan, R. & Bekyarova, E. Advances in transferring chemical vapour deposition graphene: a review. *Mater. Horizons* **4**, 1054–1063 (2017).
58. Ishigami, M., Chen, J. H., Cullen, W. G., Fuhrer, M. S. & Williams, E. D. Atomic structure of graphene on SiO₂. *Nano Lett.* **7**, 1643–1648 (2007).
59. Suk, J. W. *et al.* Enhancement of the electrical properties of graphene grown by chemical vapor deposition via controlling the effects of polymer residue. *Nano Lett.* **13**, 1462–1467 (2013).
60. Pettes, M. T., Jo, I., Yao, Z. & Shi, L. Influence of polymeric residue on the thermal conductivity of suspended bilayer graphene. *Nano Lett.* **11**, 1195–1200 (2011).
61. Chen, J.-H., Jang, C., Xiao, S., Ishigami, M. & Fuhrer, M. S. Intrinsic and extrinsic performance limits of graphene devices on SiO₂. *Nat. Nanotechnol.* **3**, 206–209 (2008).
62. Chen, J.-H. *et al.* Charged-impurity scattering in graphene. *Nat. Phys.* **4**, 377–381 (2008).
63. Pirkle, A. *et al.* The effect of chemical residues on the physical and electrical properties of chemical vapor deposited graphene transferred to SiO₂. *Appl. Phys. Lett.* **99**, 122108 (2011).
64. Ryu, S. *et al.* Atmospheric oxygen binding and hole doping in deformed graphene on a SiO₂ substrate. *Nano Lett.* **10**, 4944–4951 (2010).
65. Arjmandi-Tash, H., Jiang, L. & Schneider, G. F. Rupture index: A quantitative measure of sub-micrometer cracks in graphene. *Carbon N. Y.* **118**, 556–560 (2017).
66. Lin, W.-H. *et al.* A direct and polymer-free method for transferring graphene grown by chemical vapor deposition to any substrate. *ACS Nano*

- 8**, 1784–1791 (2014).
67. Zhang, G. *et al.* Versatile polymer-free graphene transfer method and applications. *ACS Appl. Mater. Interfaces* **8**, 8008–8016 (2016).
 68. Park, H. *et al.* Polymer-free graphene transfer for enhanced reliability of graphene field-effect transistors. *2D Mater.* **3**, 21003 (2016).
 69. Pasternak, I. *et al.* Graphene films transfer using marker-frame method. *AIP Adv.* **4**, 97133 (2014).
 70. Lima, L. M. C., Arjmandi-Tash, H. & Schneider, G. F. Lateral non-covalent clamping of graphene at the edges using a lipid scaffold. *ACS Appl. Mater. Interfaces* **10**, 11328–11332 (2018).
 71. Bekyarova, M. C. and D. S. and W. L. and B. A. and R. C. H. and E. Sublimation-assisted graphene transfer technique based on small polyaromatic hydrocarbons. *Nanotechnology* **28**, 255701 (2017).
 72. Matruglio, A. *et al.* Contamination-free suspended graphene structures by a Ti-based transfer method. *Carbon N. Y.* **103**, 305–310 (2016).
 73. Ondarçuhu, T. *et al.* Wettability of partially suspended graphene. *Sci. Rep.* **6**, 24237 (2016).
 74. Geim, A. K. & Grigorieva, I. V. Van der Waals heterostructures. *Nature* **499**, 419–425 (2013).
 75. Guinea, F., Katsnelson, M. I. & Geim, A. K. Energy gaps and a zero-field quantum Hall effect in graphene by strain engineering. *Nat. Phys.* **6**, 30–33 (2009).
 76. Pereira, V. M. & Castro Neto, A. H. Strain engineering of graphene's electronic structure. *Phys. Rev. Lett.* **103**, 46801 (2009).
 77. Bao, W. *et al.* Controlled ripple texturing of suspended graphene and ultrathin graphite membranes. *Nat. Nanotechnol.* **4**, 562–566 (2009).
 78. Wang, Y. Y. *et al.* Raman studies of monolayer graphene: the substrate effect. *J. Phys. Chem. C* **112**, 10637–10640 (2008).
 79. Lee, J. E., Ahn, G., Shim, J., Lee, Y. S. & Ryu, S. Optical separation of mechanical strain from charge doping in graphene. *Nat. Commun.* **3**, 1024 (2012).

80. Bendiab, N. *et al.* Unravelling external perturbation effects on the optical phonon response of graphene. *J. Raman Spectrosc.* **49**, 130–145 (2018).
81. Shioya, H., Russo, S., Yamamoto, M., Craciun, M. F. & Tarucha, S. Electron states of uniaxially strained graphene. *Nano Lett.* **15**, 7943–7948 (2015).
82. Bao, W. *et al.* Controlled ripple texturing of suspended graphene and ultrathin graphite membranes. *Nat. Nanotechnol.* **4**, 562–566 (2009).
83. Yoon, D., Son, Y.-W. & Cheong, H. Negative thermal expansion coefficient of graphene measured by Raman spectroscopy. *Nano Lett.* **11**, 3227–3231 (2011).
84. Lee, Y. R., Huang, J. X., Lin, J. C. & Lee, J. R. Study of the substrate-induced strain of as-grown graphene on Cu(100) using temperature-dependent Raman spectroscopy: estimating the mode Grüneisen parameter with temperature. *J. Phys. Chem. C* **121**, 27427–27436 (2017).
85. Casiraghi, C., Pisana, S., Novoselov, K. S., Geim, A. K. & Ferrari, A. C. Raman fingerprint of charged impurities in graphene. *Appl. Phys. Lett.* **91**, 233108 (2007).
86. Parobek, D. & Liu, H. Wettability of graphene. *2D Mater.* **2**, 32001 (2015).
87. de Gennes, P. G. Wetting: statics and dynamics. *Rev. Mod. Phys.* **57**, 827–863 (1985).
88. Bonn, D., Eggers, J., Indekeu, J., Meunier, J. & Rolley, E. Wetting and spreading. *Rev. Mod. Phys.* **81**, 739–805 (2009).
89. Leenaerts, O., Partoens, B. & Peeters, F. M. Water on graphene: Hydrophobicity and dipole moment using density functional theory. *Phys. Rev. B* **79**, 235440 (2009).
90. Bera, B. *et al.* Wetting of water on graphene nanopowders of different thicknesses. *Appl. Phys. Lett.* **112**, 1–6 (2018).
91. Taherian, F., Marcon, V., Van Der Vegt, N. F. A. & Leroy, F. What is the contact angle of water on graphene? *Langmuir* **29**, 1457–1465 (2013).
92. Raj, R., Maroo, S. C. & Wang, E. N. Wettability of graphene. *Nano Lett.* **13**, 1509–1515 (2013).
93. Rafiee, J. *et al.* Wetting transparency of graphene. *Nat. Mater.* **11**, 217–

- 222 (2012).
94. Driskill, J., Vanzo, D., Bratko, D. & Luzar, A. Wetting transparency of graphene in water. *J. Chem. Phys.* **141**, 18C517 (2014).
 95. Shih, C. J. *et al.* Breakdown in the wetting transparency of graphene. *Phys. Rev. Lett.* **109**, 176101 (2012).
 96. Du, F., Huang, J., Duan, H., Xiong, C. & Wang, J. Wetting transparency of supported graphene is regulated by polarities of liquids and substrates. *Appl. Surf. Sci.* **454**, 249–255 (2018).
 97. Wang, Q. H. *et al.* Understanding and controlling the substrate effect on graphene electron-transfer chemistry via reactivity imprint lithography. *Nat. Chem.* **4**, 724–732 (2012).
 98. Kozbial, A. *et al.* Study on the surface energy of graphene by contact angle measurements. *Langmuir* **30**, 8598–606 (2014).
 99. Kim, D., Pugno, N. M., Buehler, M. J. & Ryu, S. Solving the controversy on the wetting transparency of graphene. *Sci. Rep.* **5**, 15526 (2015).
 100. Shin, Y. J. *et al.* Surface-energy engineering of graphene. *Langmuir* **26**, 3798–3802 (2010).
 101. Liu, J., Lai, C.-Y., Zhang, Y.-Y., Chiesa, M. & Pantelides, S. T. Water wettability of graphene: interplay between the interfacial water structure and the electronic structure. *RSC Adv.* **8**, 16918–16926 (2018).
 102. Hong, G. *et al.* On the mechanism of hydrophilicity of graphene. *Nano Lett.* **16**, 4447–4453 (2016).
 103. Ashraf, A. *et al.* Doping-induced tunable wettability and adhesion of graphene. *Nano Lett.* **16**, 4708–4712 (2016).
 104. Shams, S. S., Zhang, R. & Zhu, J. Graphene synthesis: A Review. *Mater. Sci.* **33**, 566–578 (2015).
 105. Lee, H. C. *et al.* Review of the synthesis, transfer, characterization and growth mechanisms of single and multilayer graphene. *RSC Adv.* **7**, 15644–15693 (2017).
 106. Li, Z. *et al.* Effect of airborne contaminants on the wettability of supported graphene and graphite. *Nat. Mater.* **12**, 925–931 (2013).

107. Kimmel, G. A. *et al.* No confinement needed: observation of a metastable hydrophobic wetting two-layer ice on graphene. *J. Am. Chem. Soc.* **131**, 12838–12844 (2009).
108. Chakradhar, A., Trettel, K. & Burghaus, U. Benzene adsorption on Ru(0001) and graphene/Ru(0001)—How to synthesize epitaxial graphene without STM or LEED? *Chem. Phys. Lett.* **590**, 146–152 (2013).
109. Smith, R. S., Matthiesen, J. & Kay, B. D. Desorption kinetics of methanol, ethanol, and water from graphene. *J. Phys. Chem. A* **118**, 8242–8250 (2014).
110. Chakradhar, A. & Burghaus, U. Adsorption of water on graphene/Ru(0001)—an experimental ultra-high vacuum study. *Chem. Commun.* **50**, 7698–7701 (2014).
111. Smith, R. S., May, R. A. & Kay, B. D. Desorption kinetics of Ar, Kr, Xe, N₂, O₂, CO, methane, ethane, and propane from graphene and amorphous solid water surfaces. *J. Phys. Chem. B* **120**, 1979–1987 (2016).
112. Smith, R. S. & Kay, B. D. Desorption kinetics of benzene and cyclohexane from a graphene surface. *J. Phys. Chem. B* **122**, 587–594 (2018).
113. Sivapragasam, N., Nayakasinghe, M. T., Chakradhar, A. & Burghaus, U. Effects of the support on the desorption kinetics of n-pentane from graphene: an ultrahigh vacuum adsorption study. *J. Vac. Sci. Technol. A* **35**, 61404 (2017).
114. Wang, S., Zhang, Y., Abidi, N. & Cabrales, L. Wettability and surface free energy of graphene films. *Langmuir* **25**, 11078–11081 (2009).
115. van Engers, C. D. *et al.* Direct measurement of the surface energy of graphene. *Nano Lett.* **17**, 3815–3821 (2017).
116. Su, R. & Zhang, X. Wettability and surface free energy analyses of monolayer graphene. *J. Therm. Sci.* **27**, 359–363 (2018).
117. Spanu, L., Sorella, S. & Galli, G. Nature and strength of interlayer binding in graphite. *Phys. Rev. Lett.* **103**, 196401 (2009).
118. Björkman, T., Gulans, A., Krasheninnikov, A. V & Nieminen, R. M. van der Waals bonding in layered compounds from advanced density-functional first-principles calculations. *Phys. Rev. Lett.* **108**, 235502 (2012).

119. Van Oss, C. J., Roberts, M. J., Good, R. J. & Chaudhury, M. K. Determination of the apolar component of the surface tension of water by contact angle measurements on gels. *Colloids and Surfaces* **23**, 369–373 (1987).
120. Fowkes, F. M. Attractive forces at interfaces. *Ind. Eng. Chem.* **56**, 40–52 (1964).
121. Owens, D. K. & Wendt, R. C. Estimation of the surface free energy of polymers. *J. Appl. Polym. Sci.* **13**, 1741–1747 (1969).
122. Li, D. & Neumann, A. W. Contact angles on hydrophobic solid surfaces and their interpretation. *J. Colloid Interface Sci.* **148**, 190–200 (1992).
123. Li, D. & Neumann, A. W. Equilibrium of capillary systems with an elastic liquid-vapor interface. *Langmuir* **9**, 50–54 (1993).
124. Neumann, A. W., Good, R. J., Hope, C. J. & Sejpal, M. An equation-of-state approach to determine surface tensions of low-energy solids from contact angles. *J. Colloid Interface Sci.* **49**, 291–304 (1974).
125. Annamalai, M. *et al.* Surface energy and wettability of van der Waals structures. *Nanoscale* **8**, 5764–5770 (2016).
126. Andrews, J. E., Wang, Y., Sinha, S., Chung, P. W. & Das, S. Roughness-induced chemical heterogeneity leads to large hydrophobicity in wetting-translucent nanostructures. *Nano Lett.* **19**, 27421–27434 (2018).
127. Scocchi, G., Sergi, D., D’Angelo, C. & Ortona, A. Wetting and contact-line effects for spherical and cylindrical droplets on graphene layers: a comparative molecular-dynamics investigation. *Phys. Rev. E* **84**, 61602 (2011).
128. Andrews, J. E., Sinha, S., Chung, P. W. & Das, S. Wetting dynamics of a water nanodrop on graphene. *Phys. Chem. Chem. Phys.* **18**, 23482–23493 (2016).
129. Yiapanis, G., Makarucha, A. J., Baldauf, J. S. & Downton, M. T. Simulations of graphitic nanoparticles at air-water interfaces. *Nanoscale* **8**, 19620–19628 (2016).
130. Schrader, M. E. Ultrahigh vacuum techniques in the measurement of contact angles. IV. Water on graphite (0001). *J. Phys. Chem.* **79**, 2508–

- 2515 (1975).
131. Martinez-Martin, D. *et al.* Atmospheric contaminants on graphitic surfaces. *Carbon N. Y.* **61**, 33–39 (2013).
 132. Wehling, T. O., Lichtenstein, A. I. & Katsnelson, M. I. First-principles studies of water adsorption on graphene: the role of the substrate. *Appl. Phys. Lett.* **93**, 202110 (2008).
 133. Sengupta, S., Nichols, N. S., Del Maestro, A. & Kotov, V. N. Theory of liquid film growth and wetting instabilities on graphene. *Phys. Rev. Lett.* **120**, 236802 (2018).
 134. Ashraf, A. *et al.* Spectroscopic investigation of the wettability of multilayer graphene using highly ordered pyrolytic graphite as a model material. *Langmuir* **30**, 12827–12836 (2014).
 135. Amadei, C. A., Lai, C.-Y., Heskes, D. & Chiesa, M. Time dependent wettability of graphite upon ambient exposure: The role of water adsorption. *J. Chem. Phys.* **141**, 84709 (2014).
 136. Lai, C.-Y. *et al.* A nanoscopic approach to studying evolution in graphene wettability. *Carbon N. Y.* **80**, 784–792 (2014).
 137. Aria, A. I. *et al.* Time evolution of the wettability of supported graphene under ambient air exposure. *J. Phys. Chem. C* **120**, 2215–2224 (2016).
 138. Kozbial, A. *et al.* Understanding the intrinsic water wettability of graphite. *Carbon N. Y.* **74**, 218–225 (2014).
 139. Cunge, G. *et al.* Dry efficient cleaning of poly-methyl-methacrylate residues from graphene with high-density H₂ and H₂-N₂ plasmas. *J. Appl. Phys.* **118**, 123302 (2015).
 140. Li, Z. *et al.* Water protects graphitic surface from airborne hydrocarbon contamination. *ACS Nano* **10**, 349–359 (2016).
 141. Xue, R., Abidi, I. & Luo, Z. Domain size, layer number and morphology control for graphene grown by chemical vapor deposition. *Funct. Mater. Lett.* **10**, 1730003 (2017).
 142. Feng, X., Maier, S. & Salmeron, M. Water splits epitaxial graphene and intercalates. *J. Am. Chem. Soc.* **134**, 5662–5668 (2012).

143. Wang, Y., Sinha, S., Hu, L. & Das, S. Interaction between a water drop and holey graphene: retarded imbibition and generation of novel water-graphene wetting states. *Nano Lett.* **5**, 3815–3821 (2017).
144. Hallam, T., Berner, N. C., Yim, C. & Duesberg, G. S. Strain, bubbles, dirt, and folds: a study of graphene polymer-assisted transfer. *Adv. Mater. Interfaces* **1**, 1400115 (2014).
145. Belyaeva, L. A., van Deursen, P. M. G., Barbetsea, K. I. & Schneider, G. F. Hydrophilicity of graphene in water through transparency to polar and dispersive interactions. *Adv. Mater.* **30**, 1–7 (2018).
146. Su, Y. *et al.* Polymer adsorption on graphite and CVD graphene surfaces studied by surface-specific vibrational spectroscopy. *Nano Lett.* **15**, 6501–6505 (2015).
147. Han, Y. *et al.* Clean surface transfer of graphene films via an effective sandwich method for organic light-emitting diode applications. *J. Mater. Chem. C* **2**, 201–207 (2014).
148. Kumar, K., Kim, Y.-S. & Yang, E.-H. The influence of thermal annealing to remove polymeric residue on the electronic doping and morphological characteristics of graphene. *Carbon N. Y.* **65**, 35–45 (2013).
149. Chakradhar, A., Sivapragasam, N., Nayakasinghe, M. T. & Burghaus, U. Support effects in the adsorption of water on CVD graphene: an ultra-high vacuum adsorption study. *Chem. Commun.* **51**, 11463–11466 (2015).
150. Chakradhar, A., Sivapragasam, N., Nayakasinghe, M. T. & Burghaus, U. Adsorption kinetics of benzene on graphene: an ultrahigh vacuum study. *J. Vac. Sci. Technol. A Vacuum, Surfaces, Film.* **34**, 21402 (2016).
151. Sivapragasam, N., Nayakasinghe, M. T. & Burghaus, U. Adsorption of n-butane on graphene/Ru(0001)—a molecular beam scattering study. *J. Vac. Sci. Technol. A* **34**, 41404 (2016).
152. King, D. A. Thermal desorption from metal surfaces: A review. *Surf. Sci.* **47**, 384–402 (1975).
153. Ceyer, S. T. New mechanisms for chemistry at surfaces. *Science* **249**, 133–139 (1990).
154. Ulbricht, H., Zacharia, R., Cindir, N. & Hertel, T. Thermal desorption of

- gases and solvents from graphite and carbon nanotube surfaces. *Carbon N. Y.* **44**, 2931–2942 (2006).
155. Zangi, R. Water confined to a slab geometry: a review of recent computer simulation studies. *J. Phys. Condens. Matter* **16**, S5371 (2004).
 156. Giovambattista, N., Rosky, P. J. & Debenedetti, P. G. Phase transitions induced by nanoconfinement in liquid water. *Phys. Rev. Lett.* **102**, 50603 (2009).
 157. Daschbach, J. L., Peden, B. M., Smith, R. S. & Kay, B. D. Adsorption, desorption, and clustering of H₂O on Pt(111). *J. Chem. Phys.* **120**, 1516–1523 (2004).
 158. Ulbricht, H., Zacharia, R., Cindir, N. & Hertel, T. Thermal desorption of gases and solvents from graphite and carbon nanotube surfaces. *Carbon N. Y.* **44**, 2931–2942 (2006).
 159. Brown, W. A. & Bolina, A. S. Fundamental data on the desorption of pure interstellar ices. *Mon. Not. R. Astron. Soc.* **374**, 1006–1014 (2007).
 160. Bolina, A. S., Wolff, A. J. & Brown, W. A. Reflection absorption infrared spectroscopy and temperature-programmed desorption studies of the adsorption and desorption of amorphous and crystalline water on a graphite surface. *J. Phys. Chem. B* **109**, 16836–16845 (2005).